



# Multiple solutions and stability of confined convective and swirling flows – a continuing challenge

Multiple  
solutions and  
stability

213

Alexander Yu. Gelfgat

*Department of Fluid Mechanics and Heat Transfer,  
Faculty of Engineering, Tel-Aviv University, Tel-Aviv, Israel*

Pinhas Z. Bar-Yoseph

*Computational Mechanics Laboratory,  
Faculty of Mechanical Engineering,  
Technion – Israel Institute of Technology, Haifa, Israel*

Received August 2002

Revised January 2003

Accepted February 2003

**Keywords** Thermal stability, Finite volume methods, Rotational motion

**Abstract** Our recent results on stability and multiplicity of flow states for confined flows of an incompressible Newtonian fluid are surveyed. The considered laminar flows are caused by either thermal, mechanical, or electromagnetic effects and beyond the stability limit exhibit multiplicity of stable, steady or oscillatory, asymptotic states. Stability diagrams as well as examples of multiple flow states are given. It is concluded that beyond the critical value of the characteristic non-dimensional parameter, and below the threshold to stochastic or turbulent state, multiple stable asymptotic flow states can be expected. This means that at such flow regimes, any computational (experimental) result may be strongly dependent on its initial condition and/or computational (experimental) path. Uncertainties of experimental and numerical modeling, which follow from this conclusion, are discussed. The global spectral Galerkin method using divergence free basis functions has been employed for the spatial approximation of the velocity and temperature fields. Several numerical experiments were performed comparing the present and other formulations, each of which confirmed the computational efficiency of the present approach over other classical numerical methods.

## 1. Introduction

Fluid flow is extremely important in a wide variety of materials processing because it determines the quality and characteristics of the final product and allows control and optimization of the system. For example, flow patterns that arise in the molten material in crystal growing strongly affect the quality of the

---

This paper was presented as a keynote lecture at the *5th World Congress on Computational Mechanics*, Vienna, Austria on 7-12 July 2002.

This research was supported by the Israel Ministry of Immigrant Absorption (to A. Gelfgat), the Israel High Performance Computer Unit, Norman and Helen Asher Space Research Institute, the Fund for the Promotion of Research at the Technion, and by the Winograd Chair of Fluid Mechanics and Heat Transfer at Technion.



crystal and thus, of the semiconductors fabricated from that crystal (Jaluria, 2001). Transport phenomena in these processes are quite complex due to free, forced and Marangoni convection mechanisms which are coupled with radiation, melt-crystal interface dynamics, turbulence and free surface modeling, impurities and dopant distributions, and so on.

This review paper is mainly concerned with flow multiplicity and instability which may strongly influence the quality and structure of the final product in material processing. Interest lies mainly in the basic fluid phenomena, rather than in the complexities of the different processes. It has been clearly shown that despite the simplicity in the domain geometry and the assumption that the flow remains laminar, complicated, multiple flow patterns are revealed in all cases we have experienced. The complexity of laminar flow patterns is observed with the increase of the characteristic parameters, where the flow undergoes different bifurcations, among which the most typical are Hopf bifurcations, turning points and breaking of symmetries (reflectional, rotational, axial).

Nowadays, high performance computing units allow simulating realistic unsteady flow problems such as flows with turbulence modeling, chemical reactions, and surface tension within complicated geometric domains through employing various time marching algorithms. Yet, reliable stability and/or bifurcation analysis for such problems is not feasible due to the large dimension of the corresponding eigen problem.

Our main objectives in analyzing the stability and multiplicity of flow states are three fold.

- (1) To verify our computational approach against other independent solutions and to test its accuracy and computational efficiency.
- (2) To reveal the richness of some *basic* laminar flow states (confined in *simple* geometric domains) via a thorough computational study.
- (3) To obtain a better insight about the development of stability and multiplicity of flow states. This can serve to stimulate innovations as well as may lead to improvements in the performance, reliability and costs of many practical flow problems (e.g. crystal growth processes, rotating machines).

There are a significant number of experimental and numerical studies reporting on multiple stable laminar states, which are observed for the same values of characteristic parameters. Multiple steady states of rotating flows were reported in Albensoeder *et al.* (2001), Bartels (1982), Bar-Yoseph (1994, 1995), Bar-Yoseph *et al.* (1990, 1992), Blackburn and Lopez (2000), Cliffe and Mullin (1985), Coles (1965), Lopez *et al.* (2001a), Nore *et al.* (2003), Schrauf (1986) and Wimmer (1976). For example, Wimmer's experimental results for fluid flow between the concentric rotating spheres clearly show that the final state of the flow field depends on the initial conditions and acceleration of the inner sphere (three steady axisymmetric and two unsteady non-symmetric flow modes were

found). For flow in a wider spherical gap with thermal effects, our results (Bar-Yoseph *et al.*, 1992) show that five different flow states can be obtained, depending on the computational path in the Re-Ra plane. Multiple states in a two-sided lid-driven cavity were described by Albensoeder *et al.* (2001) and Blohm and Kuhlmann (2002), and multiple convective patterns were found by Crespo del Arco *et al.* (1989) and Pallares *et al.* (1999, 2001) (clearly, the list of examples is incomplete). Hence, it is clear that in cases of multiple stable flow states the final flow mode depends on either the initial condition and/or the computational (experimental) path. The set of all possible initial states can be divided into several regimes, each being attracted to a certain distinct asymptotic state (Wimmer, 1976). At small values of the characteristic parameter, the Navier-Stokes equation has a unique solution (Serrin, 1959). Therefore, it follows that the appearance of multiplicity of flow states can only take place at relatively large values of the characteristic parameter (at the critical value which might be below the threshold to chaos or turbulence) via flow instability.

The importance of computational modeling of bifurcation and multiplicity of fluid flows is widely understood nowadays, and special computational procedures have been extensively developed for revealing all possible bifurcations of a given solution, as well as following the corresponding branches of that solution (Cliffe *et al.*, 2000; Gaido *et al.*, 2001; Sanchez *et al.*, 2002). Yet, the computation of all possible multiple flow states, as well as the stability analysis of these computed multiple solutions, remain a challenge. To the best of our knowledge, none of the commercial CFD codes are suitable for analyzing stability and bifurcation problems. For such flow problems, the spectral method becomes very attractive because the correct pattern of the flow can be obtained with relatively few basis functions. Among the spectral methods, our approach used in the works surveyed here is the most appealing one because, unlike the other mixed methods, the present approximation of velocity field is divergence free, which yields a numerical scheme that is inherently stable (Gelfgat, 1999, 2001; Gelfgat and Tanasawa 1993, 1994; Gelfgat *et al.*, 2001c; Grants and Gerbeth, 2001; Yahata, 1999).

The present review is focused on stability and multiplicity of confined flow states caused by thermal, mechanical and electromagnetic effects, and were analyzed by our research team (Erenburg *et al.*, 2003; Gelfgat, 1999, 2001; Gelfgat and Bar-Yoseph, 2001; Gelfgat and Tanasawa 1993, 1994; Gelfgat *et al.*, 1996a-c, 1997, 1999a-c, 2000, 2001a-c). The considered problems were motivated by crystal growth (Erenburg *et al.*, 2003; Gelfgat and Bar-Yoseph, 2001; Gelfgat *et al.*, 1997, 1999a-c, 2000, 2001b), rotating machinery (Gelfgat *et al.*, 1996a-c, 2001a) and bioseparation (Gelfgat *et al.*, 2001c) applications. All results are based on the same global spectral Galerkin method (Gelfgat, 1999, 2001; Gelfgat and Tanasawa, 1993, 1994; Gelfgat *et al.*, 2001c). According to this approach, a specially constructed set of non-orthogonal basis functions, *a priori*

satisfying the continuity equation and the (linear continuous) boundary conditions, reduces the problem to the analysis of an ODEs system. The pressure is eliminated by the projection of the Navier-Stokes equations on the divergent-free basis. This enables a straightforward application of classical numerical algorithms such as the Newton iteration, arc-length continuation and standard eigenvalue solvers. The spectral, sometimes exponential, rate of convergence allows us to perform detailed parametric studies. In the following we describe the considered problems, the convergence study for some of them and the comparison with other independent studies.

As mentioned earlier, multiple flow states were observed experimentally and numerically in many other studies (Albensoeder *et al.*, 2001; Bartels, 1982; Bar-Yoseph, 1994, 1995; Bar-Yoseph *et al.*, 1990, 1992; Blackburn and Lopez, 2000; Blohm and Kuhlmann, 2002; Cliffe and Mullin, 1985; Coles, 1965; Crespo del Arco *et al.*, 1989; Lopez *et al.*, 2001a; Nore *et al.*, 2003; Pallares *et al.*, 1999, 2001; Schrauf, 1986; Wimmer, 1976). It is re-emphasized that the transition to multiplicity of solutions takes place below any threshold to chaos or turbulence. This was clearly observed in all the problems we encountered. Multiplicity has to be considered whenever comparison of independent results is made, so that the states belonging to the same solution branch are compared.

## 2. Definitions of the considered problems

We consider laminar flows of incompressible or Boussinesq, Newtonian fluids. The governing equations are the Navier-Stokes and energy equations. Thus, in the problem descriptions we define only the related boundary conditions and non-dimensional characteristic parameters.

### 2.1 Convection in a laterally-heated rectangular cavity

This problem was first studied by Batchelor (1954) and, at that time, was considered as a purely theoretical model until experiments connecting the instability of a low Prandtl fluid convection with the irregular structure of semiconductor monocrystals were reported (Hurle, 1966). In our study we focused on stability and multiplicity of steady flow states of convection in a rectangular cavity with differentially and uniformly heated vertical walls (Figure 1). The choice of the characteristic parameters was motivated by the benchmark problems defined by de Vahl Davis and Jones (1983) for convection of air in a square cavity, and by Roux (1990) for oscillatory instability of a low Prandtl number fluid convection in a cavity with aspect ratio (length/height) equal to four.

The vertical boundaries of the cavity are considered to be no-slip and isothermal, the left boundary is hot and the right one is cold. The horizontal boundaries can be considered as no-slip and perfectly thermally-insulated. The flow can be affected by an externally imposed homogeneous magnetic field  $\mathbf{B}$  of arbitrary magnitude  $B_0$  and forming an arbitrary angle  $\alpha$  with the horizontal

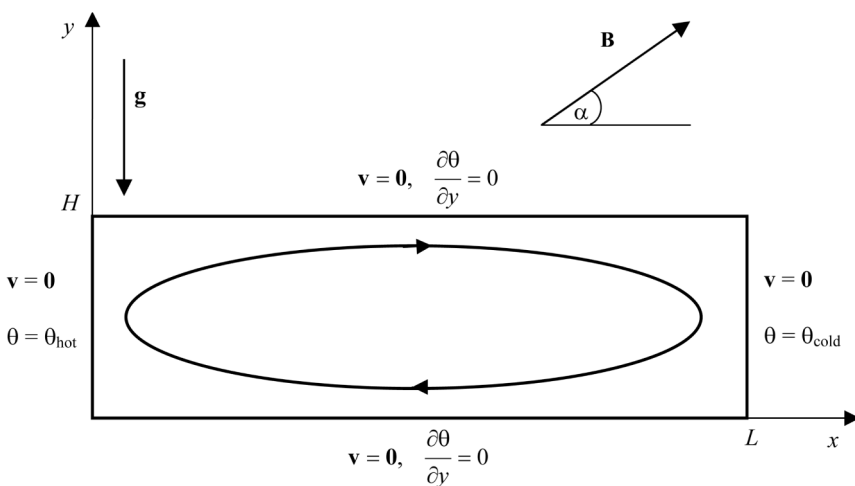


**Figure 1.**  
Buoyancy convection in  
a rectangular cavity:  
sketch of the problem  
geometry

axis. Results for other boundary conditions imposed on the horizontal boundaries (perfectly conducting boundaries, stress-free upper boundary) can be found in Gelfgat and Tanasawa (1994) and Gelfgat *et al.* (1997).

The flow is defined by the following characteristic parameters: the aspect ratio  $A = L/H$ , the Prandtl number  $\text{Pr} = \nu/\xi$ , the Grashof number  $\text{Gr} = g\beta(\theta_{\text{hot}} - \theta_{\text{cold}})H^3/\nu^2$ , and the Hartmann number  $\text{Ha} = B_0H\sqrt{\sigma}/\rho\nu$ . Here,  $L$  is the length and  $H$  the height of the cavity,  $\nu$  the kinematic viscosity,  $\xi$  the heat diffusivity,  $g$  the gravity acceleration,  $\beta$  the thermal expansion coefficient,  $\sigma$  the electric conductivity, and  $\rho$  the density.

**2.2 Rayleigh-Bénard instability in a three-dimensional box heated from below**  
This benchmark problem was formulated by Dijkstra (1998) and Gelfgat (1999), and considered as the classical Rayleigh-Bénard instability (transition from conduction to convection) in finite three-dimensional boxes with some specific boundary conditions taken from the experiments described by Koschmieder (1993). The benchmark problem was proposed for the validation of different computational methods implementing stability analysis and different continuation techniques.

A rectangular box of height  $H$ , length  $L$ , and width  $W$  is considered (Figure 2). It is assumed that all the boundaries are no-slip, except the upper one, which is stress-free. The lower boundary is uniformly heated. The vertical boundaries are thermally insulated. A convective cooling condition characterized by the Biot number  $\text{Bi}$  is imposed on the upper boundary. The other characteristic parameters are: the aspect ratios in  $x$ - and  $y$ -directions  $A_x = L/H$  and  $A_y = W/H$ , the Prandtl number  $\text{Pr} = \nu/\xi$ , and the Rayleigh number  $\text{Ra} = g\beta(\theta_{\text{hot}} - \theta_{\text{cold}})H^3/\nu\xi$ ,  $\text{Ra} = \text{Gr Pr}$ . Note that all notations are the same as defined in Section 2.1.

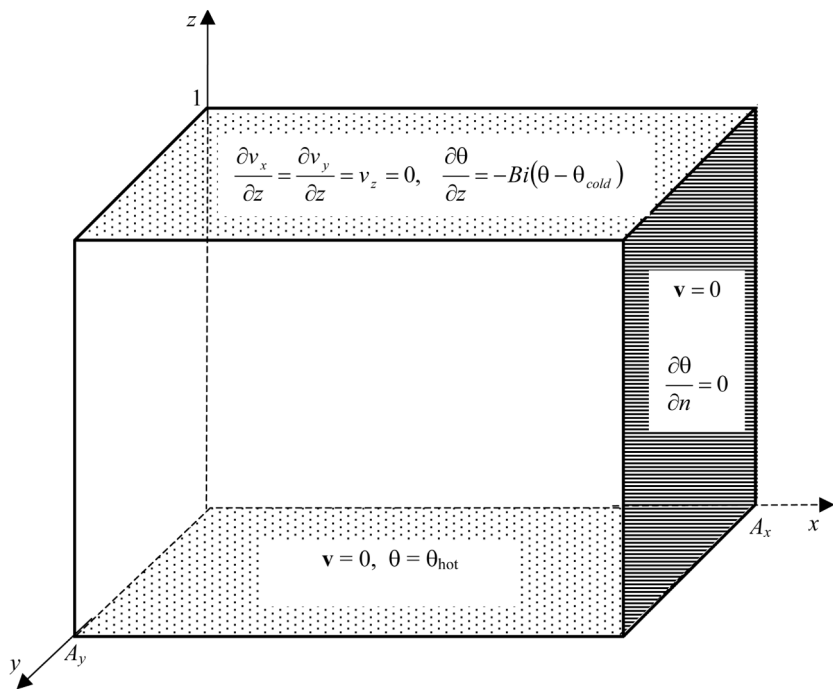


**Figure 2.**  
Rayleigh-Bénard  
instability in a 3D box:  
sketch of the problem  
geometry

The objective here is to study the dependence of the critical Rayleigh number, corresponding to the onset of convection, on both aspect ratios. Additionally, we study the patterns of the most dangerous perturbations, which qualitatively describe the supercritical convective states.

### 2.3 Convection in a cavity with partially heated sidewalls

The study of this problem was motivated by instabilities observed in the semiconductor melts during various crystal growth processes. The problem considered represents a simplified model of a case where the size of a heater is smaller than the size of the melt zone. The geometry considered relates to the floating zone and Bridgman growth techniques. It happens that this difference in sizes leads to different instability mechanisms, whose interaction creates a very complex multiplicity of possible flow states.

A natural convection flow in a cavity, whose vertical walls are uniformly heated in their central parts and are insulated above and below, is considered (Figure 3). All boundaries are assumed to be no-slip, and horizontal boundaries are maintained at a cold temperature. The problem is governed by the following characteristic parameters: the aspect ratio of the cavity  $A_L = H/L$ , the Prandtl number  $\text{Pr} = v/\xi$ , the Grashof number  $\text{Gr}_L = g\beta(\theta_{hot} - \theta_{cold})L^3/v^2$ , and the two additional geometric parameters  $\alpha_1 = h_1/L$  and  $\alpha_2 = h_2/L$  describing the location of the heated parts of the vertical walls. Note that here we use the length

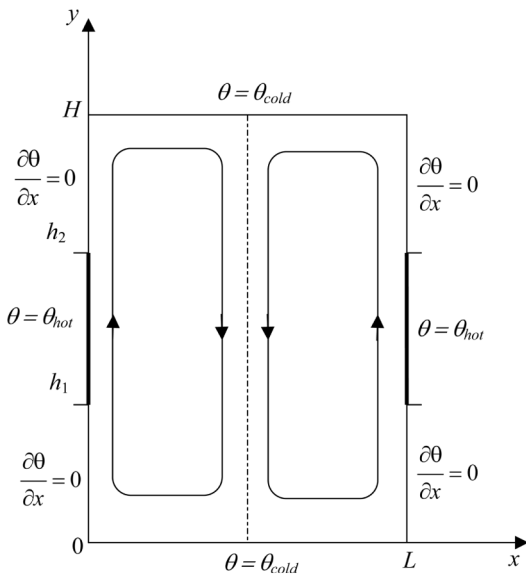


**Figure 3.**  
Natural convection in a two-dimensional cavity with partially heated vertical walls: sketch of the problem geometry

of the cavity as a characteristic length, and denote the aspect ratio and the Grashof number by a subscript  $L$  to distinguish them from those defined in Section 2.1. Other notations are exactly the same as in Section 2.1.

The values of the characteristic parameters,  $\text{Pr} = 0.021$ ,  $\alpha_1 = A_L/2 - 1/4$ ,  $\alpha_2 = A_L/2 + 1/4$ ,  $1 \leq A_L \leq 6$ , were taken from the experiments of Selver *et al.* (1998). It was unexpectedly found that such a simple configuration exhibits panoply of distinct stable and unstable, steady and oscillatory states (Erenburg *et al.*, 2003). Therefore, this problem represents a simple example, where a study of the stability and multiplicity of possible flow states cannot be completed without a computational tool specifically tailored for such a kind of analysis.

#### 2.4 Swirling flow in a cylinder with independently rotating top and bottom

Vortex breakdown in a closed circular cylinder with a rotating lid was first observed by Vogel (1975) and since that time it has been a subject of intensive experimental and theoretical investigations (Delery, 1994; Escudier, 1984). The importance of the vortex breakdown of swirling flows (Delery, 1994) led to wide interest in this particular problem, which can be investigated relatively easily both experimentally and computationally.

A swirling flow in a cylinder of height  $H$  and radius  $R$ , whose top and bottom can rotate independently, is considered (Figure 4(a)). The characteristic parameters are the aspect ratio of the cylinder  $\gamma = H/R$ , the Reynolds number defined by the angular velocity of the top cover  $\text{Re} = \Omega_{\text{top}} R^2 / v$ , and the rotation ratio  $\xi = \Omega_{\text{top}} / \Omega_{\text{bottom}}$ .

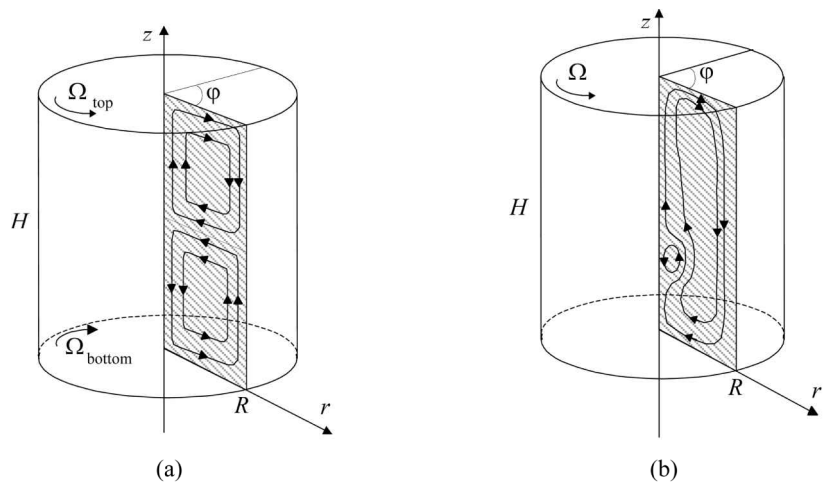


**Figure 4.**  
Swirling flow in a cylinder: sketch of the problem geometry and flow patterns

The vortex breakdown phenomenon is schematically shown in Figure 4(b). At a certain value of the Reynolds number and for  $\xi = 0$ , the main meridional vortex splits into two and a weak recirculation zone appears near the cylinder axis. Then it was shown that the vortex breakdown in this system is not caused by the instability of the flow (Gelfgat *et al.*, 1996a-c), the attention was focused on the onset of the oscillatory instability of this flow. We discuss here the convergence of the critical Reynolds numbers corresponding to axisymmetric and three-dimensional perturbations. We also discuss how the flow pattern changes with the variation of the rotation ratio  $\xi$ , and the possibility of multiple oscillatory states in supercritical flow regimes. Some of the results reported here are in excellent agreement with the results of Blackburn and Lopez (2000), Lopez *et al.* (2001a, b), Marques and Lopez (2001) and Nore *et al.* (2003), so they can be considered as the results of benchmark quality.

**2.5 Swirling flow enclosed in a cylinder and driven by a rotating magnetic field**  
A rotating magnetic field (RMF) can be used to control the flow pattern and its stability in different crystal growth processes (Dold and Benz, 1999) Besides that, this problem is directly related to confined swirling flows described in the previous section and being intensively studied nowadays.

The flow of electrically conducting fluid in a cylinder driven by a rotating magnetic field is considered (Figure 5). The flow is governed by three characteristic parameters: the aspect ratio of the cylinder,  $\gamma = H/R$ , the magnetic Taylor number  $T_{\text{am}} = B_0^2 R^4 \sigma \omega / 2 \rho v^2$  and the rotational magnetic Reynolds number  $Re_\omega = \omega R^2 / v$ . Here  $B_0$  is the magnitude and  $\omega$  is the circular frequency of rotation of the magnetic field. The other characteristic parameters are defined earlier. For details, refer Grants and Gerbeth (2001) and

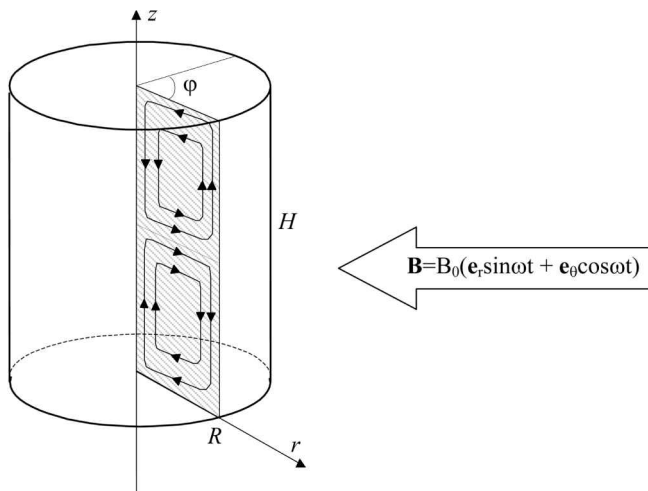


**Figure 5.**  
Swirling flow enclosed in a cylinder and driven by a rotating magnetic field: sketch of the problem geometry and flow patterns

references therein. Note that the direction of the meridional flow in Figure 5 is opposite to the one depicted in Figure 4(a).

### 2.6 Two-fluid Dean flow in a cylindrical annulus

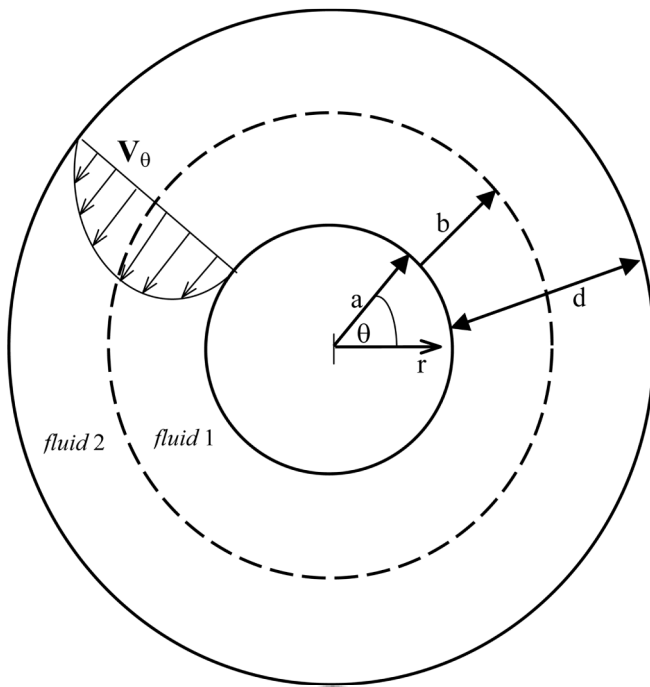
Consideration of the following problem was motivated by a search for the most effective vortical enhancement of protein diffusion through an immiscible liquid-liquid interface. Among other models we intend to consider a two-fluid flow in a helical pipe, where Dean vortices appear due to the pipe curvature (Berger and Talbot, 1983).

To obtain a better understanding of the appearance of the Dean vortices in a two-fluid system, we extended the classical Dean problem (Dean, 1928), modeling the flow in a curved channel, to the case of two immiscible fluids filling two adjacent cylindrical layers (Figure 6).

Consider a cylindrical annulus, whose radius varies in the interval  $a \leq r \leq a + d$ , filled with two immiscible Newtonian incompressible liquids 1 and 2 which, in the unperturbed state, occupy cylindrical layers  $a \leq r \leq a + b$  and  $a + b \leq r \leq a + d$ , respectively (Figure 6). It is assumed that the flow is driven by a constant azimuthal pressure gradient, i.e.  $\partial p / \partial \theta = G = \text{const}$ .

The characteristic parameters are the relative radius of curvature of the layer  $\bar{a} = a/d$ , the relative depth of the inner layer  $\bar{b} = b/d$ , the Dean number  $\text{De} = (d/\eta_1) \sqrt{G\rho_1/a}$ , and the ratios of the densities and the dynamic viscosities of the two fluids  $\rho_{21} = \rho_2/\rho_1$  and  $\eta_{21} = \eta_2/\eta_1$ , respectively. Accounting for the capillary forces on the liquid-liquid interface, the Weber number  $\text{We} = Gd/\alpha$  is also introduced. Here  $a$  is the radius of the inner cylinder,  $d$  the annulus width,  $\alpha$  the surface tension coefficient, and  $G$  the azimuthal pressure gradient.

The objective of this study is to carry out a three-dimensional linear stability analysis of the basic azimuthal flow. It appears, that conversely to the

**Figure 6.**

Two-fluid Dean flow in a cylindrical annulus:  
sketch of the problem

single-fluid case, where the instability is always two-dimensional (Dean, 1928), the instability of the two-fluid case can be two- or three-dimensional depending on the characteristic parameters. The extension of the global Galerkin method for small perturbations of the liquid-liquid interface is described in Gelfgat *et al.* (2001c).

### 2.7 Three-dimensional instability of axisymmetric convection flows

As another example of the transition from steady axisymmetric to three-dimensional (steady or oscillatory) flow we consider the three-dimensional instability of an axisymmetric convective flow within a cylinder. The problem is also motivated by the crystal growth applications, where melt flows may become three-dimensional (which is undesirable) in spite of perfectly axisymmetric forcing, geometry and boundary conditions.

It is assumed that certain axisymmetric thermal boundary conditions are defined on the cylinder boundaries, so that the base convective flow is axisymmetric (Figure 7).

The flow is defined by the aspect ratio  $\gamma = H/R$ , Prandtl number  $\text{Pr} = \nu/\xi$ , and the Grashof number  $\text{Gr} = g\beta(\theta_{\text{hot}} - \theta_{\text{cold}})R^3/\nu^2$ . The hot and cold temperatures should be defined according to certain heating conditions, which may require additional characteristic parameters. The main purpose of this

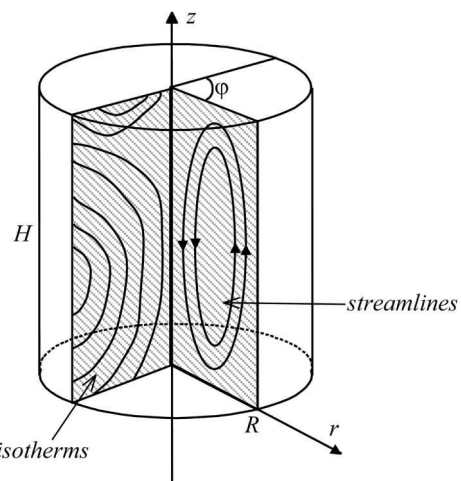


**Figure 7.**  
Axisymmetric natural  
convection flow in a  
cylinder: sketch of the  
problem

study is to find the critical values of  $\text{Gr}$  corresponding to the transition from an axisymmetric to a three-dimensional flow state.

**2.8 Three-dimensional instability of Taylor-Couette flow with axial through-flow**  
This is a classical Taylor-Couette configuration of rotating flow between the two independently rotating cylinders with an axial through-flow imposed on it (Figure 8). The problem is defined by the Taylor number  $\text{Ta} = R_i \Omega_i d / v$ ,

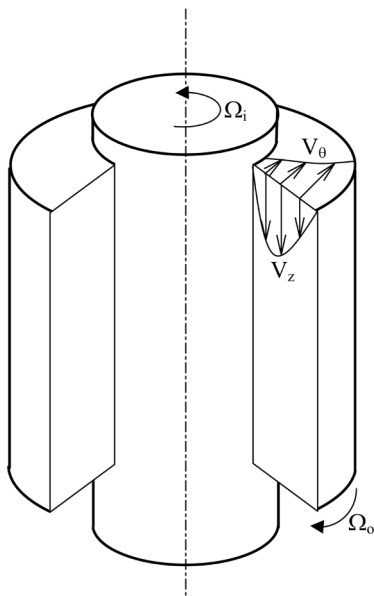


**Figure 8.**  
Taylor-Couette system  
with axial through-flow

rotation ratio  $\xi = \Omega_i/\Omega_o$ , the Reynolds number of the axial flow  $Re = Wd/v$ , and the radii ratio  $\eta = R_i/R_o$ . Here  $R_i$  and  $R_o$  are the radii of the inner and outer cylinders,  $\Omega_i$  and  $\Omega_o$  are the angular velocities of the inner and outer cylinders, respectively;  $d = R_o - R_i$  is the gap between the cylinders,  $v$  is the kinematic viscosity, and  $W$  is the mean velocity of the axial flow. The flow is assumed to be periodic in the axial direction.

Multiple three-dimensional states of the flow were experimentally observed in this system (Lueptow *et al.*, 1992). We used this configuration to validate the fully three-dimensional finite volume code.

### 3. Computational method

As mentioned earlier, the main computational method used for studying the problems defined earlier is the global Galerkin method. The divergence-free velocity basis functions satisfying all homogeneous linear boundary conditions for two-dimensional flows in Cartesian coordinates were proposed and validated by Gelfgat and Tanasawa (1994). Three-dimensional bases for Cartesian coordinates were introduced and verified by Gelfgat (1999). Axisymmetric and three-dimensional bases for cylindrical coordinates were introduced in Gelfgat and Tanasawa (1993) and then were validated in Gelfgat *et al.* (1996a, 1999c) (for details, refer Gelfgat (2001)). Different ways to handle discontinuous boundary conditions were proposed by Erenburg *et al.* (2003) and Gelfgat *et al.* (1996a, 1999c). The bases for a two-fluid case including the perturbations of a capillary liquid-liquid interface are described by Gelfgat *et al.* (2001c). Here the numerical approach is briefly described.

The unknown velocity and temperature fields,  $\mathbf{v}$  and  $\theta$ , are approximated as

$$\mathbf{v}(t, \mathbf{r}) = \mathbf{W}(\mathbf{r}) + \sum_{i=1}^N X_i(t) \mathbf{u}_i(\mathbf{r}), \quad \theta(t, \mathbf{r}) = Q(\mathbf{r}) + \sum_{i=1}^M X_{i+N}(t) g_i(\mathbf{r}) \quad (1)$$

Here  $\mathbf{u}_i$  and  $g_i$  are the bases of the velocity and temperature, respectively.  $X_i(t)$  are unknown time-dependent coefficients to be found.  $\mathbf{W}$  and  $Q$  are auxiliary functions used to satisfy inhomogeneous boundary conditions, so that all linear boundary conditions for the basis functions  $\mathbf{u}_i$  and  $g_i$  are homogeneous. The basis functions satisfy *all* the linear homogeneous boundary conditions. The velocity basis functions are *divergence-free*. For more details and examples of the basis functions, refer Gelfgat (2001).

Due to the orthogonality of the subspace of potential functions to the subspace of divergence-free functions, projection of the residuals on the basis eliminates the pressure from the Navier-Stokes equations. The resulting dynamical system can be written in the form

$$\frac{dX_i(t)}{dt} = L_{ij}X_j(t) + N_{ijk}X_j(t)X_k(t) + F_i \quad (2)$$

---

where the indices  $i, j$  and  $k$  vary from one to  $N + M$  and summation over repeating indices is assumed. The matrices  $\mathbf{L}$ ,  $\mathbf{N}$  and  $\mathbf{F}$  contain projections of all the linear, bilinear and source terms of the Navier-Stokes (or Boussinesq) equations, respectively, and depend on all the characteristic parameters of a given problem.

After calculation of the Galerkin projections is completed, the ODEs system (2) becomes the main object of the computational procedure. Steady state solutions of equation (2) are computed by the Newton iteration. The arc-length continuation is applied where necessary.

The linear stability of the computed steady solution is defined by the spectrum of the Jacobian matrix of the ODEs system (2): the solution is unstable if at least one eigenvalue  $\lambda$  with a positive real part exists. The critical characteristic parameters correspond to the appearance of the first eigenvalue changing the sign of its real part from negative to positive. After the critical value is computed, it is sometimes possible to approximate asymptotically weak supercritical states. The corresponding algorithm for the Hopf bifurcation (transition from steady to oscillatory state) can be found in Gelfgat (2001) and Gelfgat *et al.* (1996a).

The method is validated by comparison with the published numerical and experimental data, or with our own results obtained by the time-dependent finite volume code.

## 4. Results and discussion

### 4.1 Convection in a laterally heated cavity

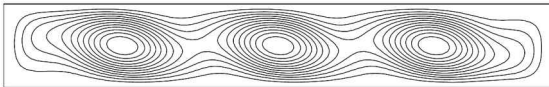
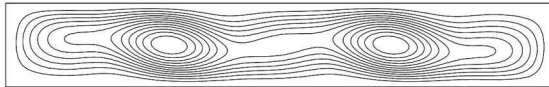
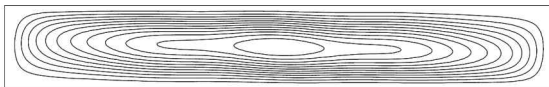
Some typical results for problem 2.1 and for different Prandtl numbers and aspect ratios are reported by Gelfgat (2001), Gelfgat and Bar-Yoseph (2001), Gelfgat and Tanasawa (1994) and Gelfgat *et al.* (1997, 1999a, b). Convergence studies and comparison with other independent computations for low Prandtl number fluids were reported by Gelfgat *et al.* (1997, 1999a, b). It was shown that the computation of the critical Grashof number up to the third or fourth decimal digit is yielded by the use of 30 basis functions in the short dimension and 60 functions in the long dimension. As expected, the convergence rate for convective flows with larger Prandtl numbers can deteriorate significantly in cases where the resolution of thin thermal boundary layers is insufficient.

Here, we focus on the multiplicity of the steady flow states which are found in long horizontal cavities with the no-slip and thermally insulated horizontal boundaries. As an example, we choose the case with  $\text{Pr} = 0$ , which means that the effect of heat convection is neglected (and is also easier for interpretation). Results for cases having non-zero Prandtl numbers can be found in Gelfgat *et al.* (1997, 1999a, b).

Three distinct steady states computed for the same set of the characteristic parameters are shown in Figure 9(a). These states were first obtained by the global Galerkin method and then were recalculated by the finite volume method. Note that all the three states are *stable*.

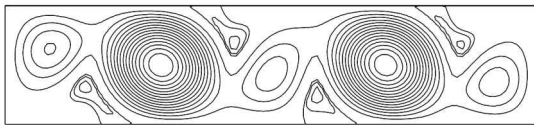
HFF  
14,2

226

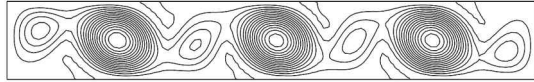


(a)

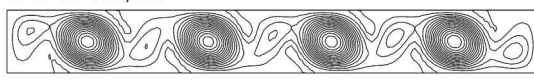
A=4.8 Gr=600,000



A=7.25 Gr=550,000



A=9 Gr=750,000



(b)

**Figure 9.**

Multiple steady states of natural convection in long horizontal cavities.  
(a) three distinct steady states at  $A = 7$ ,  $\text{Pr} = 0$ ,  $\text{Gr} = 8.8 \times 10^4$ ; and  
(b) non-symmetric steady states

For the considered boundary conditions the flow patterns are symmetric with respect to the rotation of the cavity around its center, which is the consequence of the symmetric boundary conditions (e.g. patterns shown in Figure 9(a)). This symmetry, however, can be broken through a steady pitchfork bifurcation leading to the non-symmetric patterns. These are shown in Figure 9(b). Therefore, we observe here

- (1) distinct centrally symmetric patterns characterized by different number of convective rolls (Figure 9(a)); and
- (2) non-symmetric patterns branching from the symmetric ones (Figure 9(b)).

Clearly, to describe which flow patterns are physically reachable (i.e. exists and stable) one has to investigate where a pattern exists and is it stable. This has to be done separately for each pattern. The completed study is presented as a stability diagram in Figure 10. Each symmetric pattern is stable below and inside the corresponding neutral curve. The non-symmetric states are stable inside the shaded regions. The regions where several stable steady states exist simultaneously can be easily found in Figure 10. Furthermore, above the critical curves oscillatory steady states with different number of oscillating convective rolls exist. Therefore, the final asymptotic state of the flow depends on the particular initial conditions. Based on that argument one can propose an explanation for the experimental observations of Pratte and Hart (1990) (See Gelfgat *et al.*, 1999b). In Gelfgat *et al.* (1999a) we described how each steady pattern can be reached numerically.

#### 4.2 Rayleigh-Bénard instability in a rectangular box

Results for problem 2.2 are reported in Gelfgat (1999). The corresponding convergence study showed that the critical Rayleigh number corresponding to the primary Rayleigh-Bénard instability can be computed to within three to four correct decimal digits already with the use of six basis functions in the shorter dimension and 12 functions in the longer dimension. It was revealed

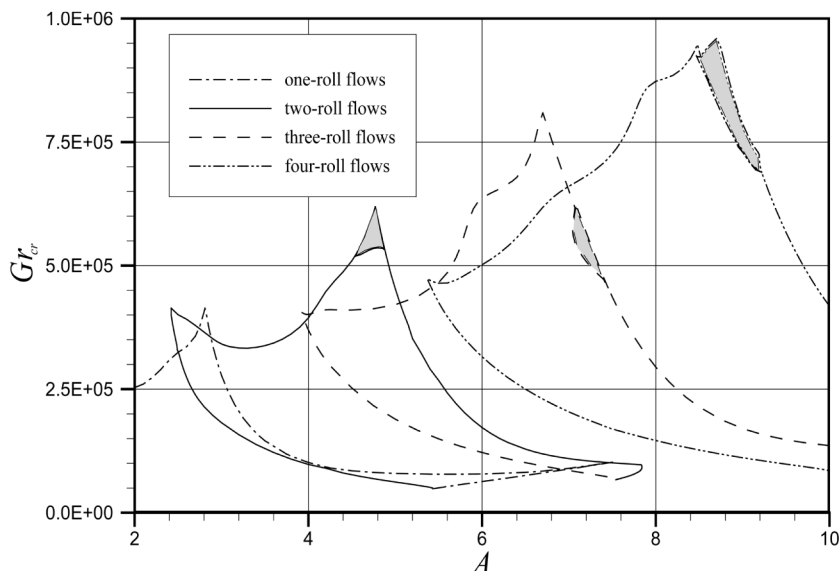


**Figure 10.**  
Stability diagram for  
 $Pr = 0$  and  $2 < A < 10$   
(Gelfgat *et al.*, 1999a).  
Symmetric flow patterns  
are stable below and  
inside the corresponding  
curves. Non-symmetric  
patterns are stable in the  
shaded regions

that there are several different patterns of Rayleigh-Bénard rolls, which can be distributed along the different horizontal directions, or to be of torus-like shape with the fluid ascending near the boundaries and descending near the center. An illustration is shown in Figure 11, where two most dangerous modes replacing each other with the variation of the aspect ratio  $A_y$  are shown (Gelfgat, 1999). The modes switch at  $A_y = 1.28$ .

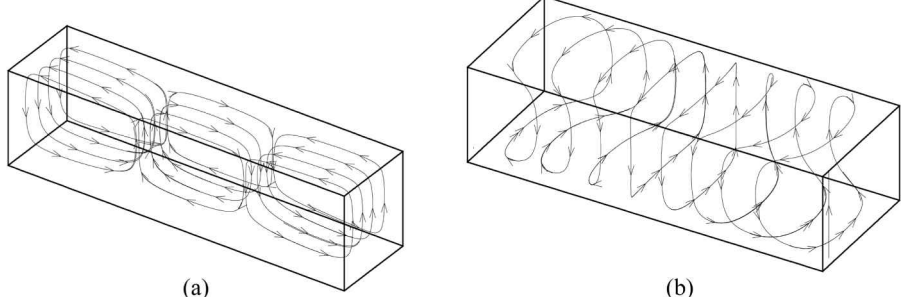
At moderate supercriticalities, several Rayleigh-Bénard modes compete, so that the final asymptotic state depends on the particular initial conditions. Seven distinct states were predicted numerically (Pallares *et al.*, 1999) and observed experimentally (Pallares *et al.*, 2001) for a supercritical Rayleigh-Bénard convection in a cubic cavity.

#### 4.3 Convection in a cavity with partially heated sidewalls

The flow in the symmetrically heated cavity is initially symmetric as shown in Figure 3. The primary instability breaks the symmetry, which takes place via steady pitchfork or Hopf bifurcation depending on the aspect ratio  $A_L$ . The supercritical steady states undergo a series of turning point bifurcations. There are intervals of the Grashof number where the existence of several steady and oscillatory states is possible. This is shown in Figure 12 for  $A_L = 6$ .

To illustrate the developing non-symmetry flow, we plot the difference of the Nusselt numbers calculated at the heated parts of the left and right boundaries,  $Nu_L$  and  $Nu_R$ , respectively, versus the Grashof number (Figure 12). With the increase of the Grashof number up to  $Gr = 1.07 \times 10^5$  (point S) the flow remains symmetric (between  $Gr = 0$  and point S). The steady symmetry-breaking bifurcation takes place at  $Gr = 1.07 \times 10^5$  (point S). As a result, a non-symmetric flow pattern develops, which is indicated by a non-zero difference of  $Nu_L - Nu_R$ . With a further increase in the Grashof number, the non-symmetric flow pattern continuously transforms into one, having the most intensive vortex in the upper part of the cavity. These flows remain stable until the Hopf bifurcation (oscillatory instability) sets in at  $Gr = 4.69 \times 10^4$  (point H). The stable branches of symmetric and non-symmetric steady states are indicated by bold lines. At larger Grashof numbers, beyond the Hopf

**Figure 11.**  
Streaklines of perturbation of velocity (Gelfgat, 1999). (a)  
 $A_x = 4$ ,  $Bi = 1$ ,  $A_y = 1$ ,  
 $Ra_{cr} = 2,645$ , and  
(b)  $A_x = 4$ ,  $Bi = 1$ ,  
 $A_y = 1.5$ ,  $Ra_{cr} = 2,043$



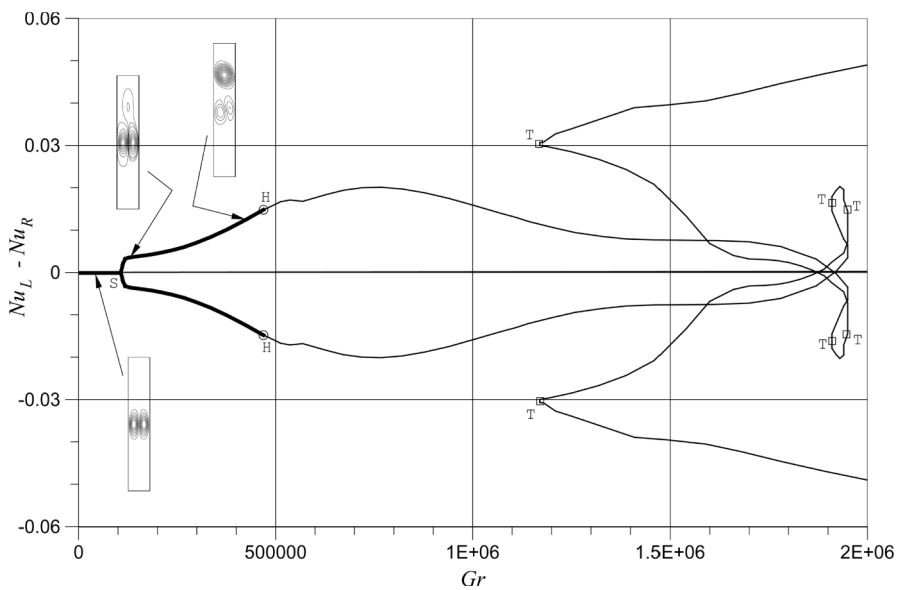


**Figure 12.**  
Bifurcation diagram for  
 $A_L = 6$

bifurcation, all steady states are oscillatory unstable. However, following the development of unstable steady states with the increase of  $Gr$ , one can find a rather complicated behavior for  $Gr > 1.2 \times 10^6$  (Figure 12). Thus, the unstable steady state branch undergoes three turning point bifurcations (at point  $T$ ), so that seven distinct steady states exist in the interval  $1.17 \times 10^6 \leq Gr \leq 1.89 \times 10^6$  and nine states in the interval  $1.91 \times 10^6 \leq Gr \leq 1.95 \times 10^6$ . As mentioned, all the steady states are oscillatory unstable. Thus, around each unstable steady branch, a stable or unstable limit cycle exists, which means the multiplicity of oscillatory flow states.

#### 4.4 Swirling flow in a cylinder with independently rotating top and bottom

Linear stability analysis for an axisymmetric flow in a cylinder with rotating top and stationary bottom was reported for the first time in Gelfgat *et al.* (1996a). In that study, the dependence of the critical Reynolds number  $Re_{cr}$  on the aspect ratio for *axisymmetric* perturbations was presented. In particular, it was shown that the appearance and disappearance of the vortex breakdown are not connected with the stability of the flow, and that the instability onset is not connected with the vortex breakdown phenomenon. A similar study for a cylinder with independently rotating top and bottom was carried out by Gelfgat *et al.* (1996b). In that work, changes in steady flow patterns that occur with a variation of the rotation ratio  $\xi$ , and the dependence  $Re_{cr}(\xi)$  for  $\gamma = 1.5$  were presented. A stability diagram for  $\xi = 1$  was reported by Gelfgat *et al.* (1996c).

An example of the change of the flow pattern with the variation of the rotation ratio  $\xi$  is shown in Figure 13. Following the above examples one may

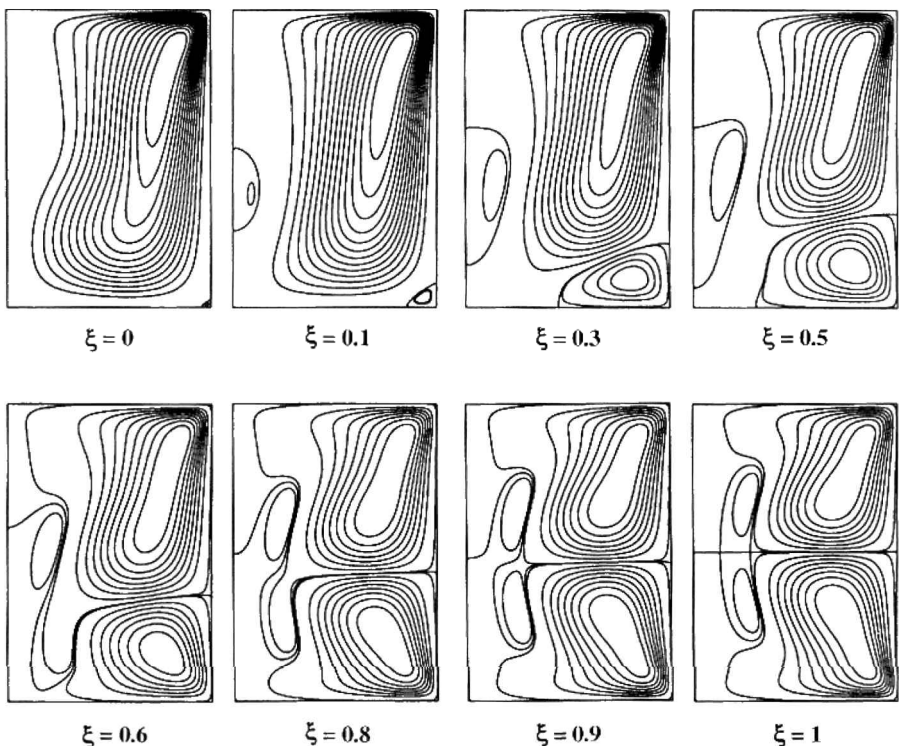


**Figure 13.**  
Cylinder with co-rotating top and bottom:  
streamlines of the  
axisymmetric meridional  
flow.  $Re = 1,000$ ,  $\gamma = 1.5$   
(the left vertical  
boundary coincides with  
the axis of symmetry)

assume that the patterns corresponding to  $\xi = 0$  and  $1$  belong to different solution branches. However, from Figure 13 we see that, with the variation of  $\xi$ , the flow continuously transforms from one flow state to another, and therefore no multiplicity of solutions is observed. Similar changes of the flow pattern can be observed also for other aspect ratios (Gelfgat *et al.*, 1996b). Does Figure 13 provide a counter example to the multiplicity of the convective flow discussed earlier? Not exactly, since the multiplicity of stable asymptotic states for this swirling flow is observed in the axisymmetric oscillatory regime (Lopez *et al.*, 2001a, b) beyond the steady-oscillatory transition studied by Gelfgat *et al.* (1996a-c, 2001a).

A fully three-dimensional linear stability analysis was performed by Gelfgat *et al.* (2001a) for  $\xi = 0$ . It was shown that the instability is three-dimensional for  $\gamma < 1.63$  and  $\gamma > 2.76$ , but remains axisymmetric in the interval  $1.63 < \gamma < 2.76$ . Here, we show a few examples obtained by Gelfgat *et al.* (1996a-c, 2001a) and compare the computed critical Reynolds numbers with those reported later by other authors.

The possibility of having multiple three-dimensional oscillatory states follows also from the results of our three-dimensional stability analysis. To illustrate this, we show a fragment of the stability diagram for  $2.5 < \gamma < 3.5$

in Figure 14. Using the  $2\pi$ -periodicity in the azimuthal direction  $\theta$  the three-dimensional perturbation is approximated via the Fourier series expansion, so that the linear stability problem separates for each  $k$ th Fourier mode. The latter is expressed as  $A(r,z)\exp(ik\theta + \lambda t)$  (Gelfgat, 2001; Gelfgat and Tanasawa, 1993; Gelfgat *et al.*, 2001a). Multiple states can be expected in the region of hysteresis, which is observed for  $3.3 < \gamma < 3.4$  and  $k = 3$ . Also for large supercriticalities, say for  $\text{Re} > 3,500$ , several unstable modes can develop and interact, thus leading to multiple oscillatory supercritical states. For example, such two distinct three-dimensional oscillatory states were observed by Blackburn and Lopez (2000) for  $\gamma = 2.5$  and  $k = 5$  and 6, while the most unstable Fourier mode at this aspect ratio is axisymmetric. Multiple three-dimensional oscillatory solutions were calculated also in the cylinder with  $\gamma = 1$  and co-rotating top and bottom ( $\xi = 1$ ) (Nore *et al.*, 2003). Secondary bifurcations caused by an interaction of different three-dimensional modes were found in Blackburn and Lopez (2000), Lopez *et al.* (2002) and Nore *et al.* (2003). To summarize, we conclude that beyond a certain supercritical value of the Reynolds number, the considered swirling flow exhibits a multiplicity of axisymmetric and three-dimensional oscillatory states. As for the problems described earlier, the final asymptotic state depends on the particular initial conditions.

Table I compares the critical Reynolds number calculated by our numerical approach with several independent calculations. It is seen that our results, obtained with  $30 \times 30$  to  $40 \times 40$  basis functions, can be reproduced on rather

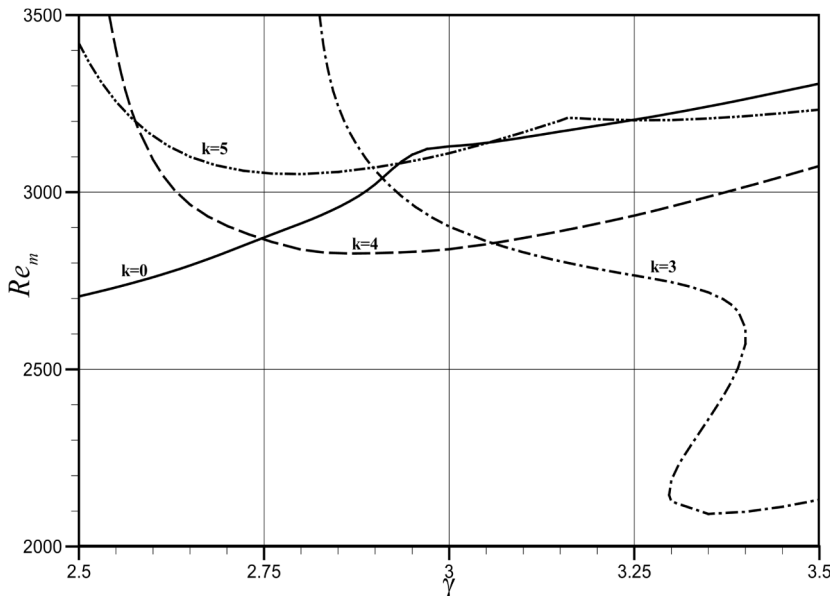


**Figure 14.**  
Fragment of the stability  
diagram for swirling  
flow in a cylinder with  
rotating top. The 3D  
perturbation is defined  
as  $A(r,z)\exp(ik\theta + \lambda t)$

fine grids with about  $200 \times 200$  nodes of finite difference discretization (Lopez *et al.*, 2001a; Nore *et al.*, 2003). The feasibility of parametric stability analysis is determined by a drastic reduction in the number of degrees of freedom provided by the spectral method. A pseudospectral method, like the one used by Marques and Lopez (2001) and Lopez *et al.* (2002) yields good accuracy with fewer number of degrees of freedom (than the finite difference method), but uses a pressure-correction procedure for time-marching and therefore does not seem to be suitable for the stability analysis. This comparison validates our stability results for the considered swirling flow. It should be emphasized that the low dimension of our approximation allows us to perform a parametric study of stability. This does not seem feasible with other numerical techniques.

#### 4.5 Swirling flow enclosed in a cylinder and driven by a RMF

Here, we report on some preliminary results obtained during our ongoing investigation. We consider the case when the Lorenz force is negligibly small compared to the time-averaged RMF force. This corresponds to the limit  $Re_\omega \rightarrow \infty$ . Three distinct patterns of steady flows are shown in Figure 15. The pattern shown in Figure 15(a) is stable while the other two are unstable. The two symmetric patterns, shown in Figure 15(a) and (b), were already reported by Grants and Gerbeth (2001). Our conclusion that the one shown in Figure 15(a) is stable while the other one in Figure 15(b) is unstable is in agreement with the results of Grants and Gerbeth (2001). The non-symmetric steady pattern shown in Figure 15(c) is reported here for the first time. Obviously, the non-symmetric patterns develop via a symmetry-breaking pitchfork bifurcation, so that there are two equivalent non-symmetric solutions. Our preliminary results show that for  $Ta_m > 10^5$  there are stable limit cycles around the unstable steady states (Figures 15(a) and (b)). However, it is yet to be checked whether these limit cycles are stable or unstable.

This problem is very attractive because it can be easily reproduced in experiment, has no discontinuities in the boundary conditions (conversely to problem 2.4) and has direct practical applications (stirring of liquid metal and

$\gamma:k$	Parameters		Critical Reynolds number	Discretization, $N_r \times N_z$	
	Present	Independent	Present	Independent	
2.5:0	2,706	2,707 (Lopez <i>et al.</i> , 2001b)	30 × 30	140 × 350 uniform grid, finite difference	
1:2	2,471	2,473 (Nore <i>et al.</i> , 2003)	40 × 40	200 × 200 uniform grid, finite difference	
3:4	2,839	< 2,850 (Marques and Lopez, 2001)	40 × 40	64 × 64 Legendre pseudospectral	
3.5:3	2,132	< 2,150 (Marques and Lopez, 2001)	40 × 40	64 × 64 Legendre pseudospectral	

**Table I.**  
Critical Reynolds number for swirling flow within a cylinder with rotating top and stationary bottom ( $\xi = 0$ )

control of liquid metal flows) (Berelowitz and Bar-Yoseph, 1992; Dold and Benz, 1999). Study of axisymmetric stability of this flow was initiated by Grants and Gerbeth (2001). The three-dimensional stability analysis is yet to be carried out. The combination of the RMF and convective effects can be considered as a possible extension of this problem.

#### 4.6 Two-fluid Dean flow in a cylindrical annulus

To solve this problem, it was necessary to extend our numerical technique to include the boundary conditions on the liquid-liquid interface in the continuous Galerkin basis. Besides this we proposed an extension which allows us to account for small perturbations of the interface considering its capillary properties. Details of these extensions and the main results are described by Gelfgat *et al.* (2001c). It is emphasized that these extensions can be used also for stability analysis of other two-fluid configurations, such as two-layer Rayleigh-Bénard (Fujimura and Renardy, 1995), Taylor-Couette (Renardy and Joseph, 1985) or plane Couette (Li and Renardy, 1998) flows.

The problem is  $2\pi$ -periodic in the azimuthal direction, and has the translational symmetry in the axial direction, and therefore the perturbation can be expressed as  $A(r)\exp(ik\theta + i\alpha z + \lambda t)$ , for an integer azimuthal wavenumber  $k$  and a real axial wavenumber  $\alpha$ . The marginal Dean number value is defined by the equation  $\text{Real}[\lambda(\text{De}_m)] = 0$  for fixed  $k$  and  $\alpha$ . The critical Dean number is the minimum of the marginal numbers over all possible values of  $k$  and  $\alpha$ .

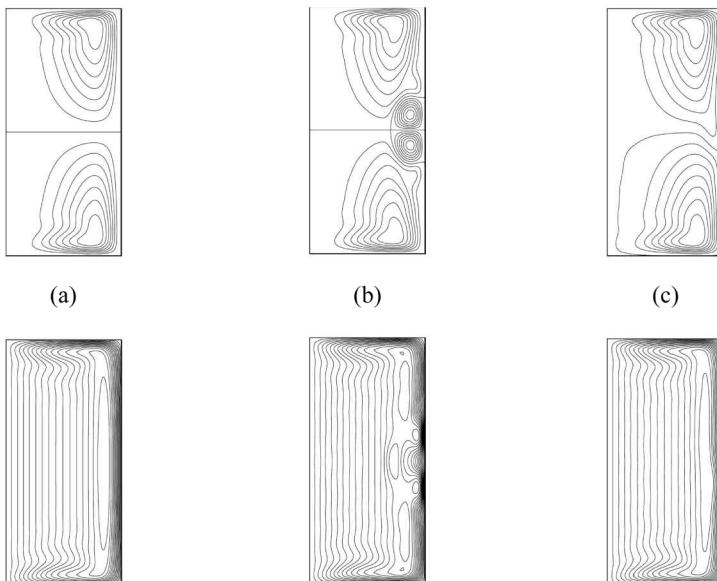


**Figure 15.**  
Streamlines of  
meridional flows (upper  
frames) and isolines of  
azimuthal velocity (lower  
frames) for three multiple  
states of the swirling  
flow driven by a rotating  
magnetic field.  $\gamma = 2$ ,  
 $T_{am} = 10^5$ ,  $Re_\omega = \infty$   
(Lorenz force effect is  
neglected). The fourth  
non-symmetric state can  
be obtained by turning  
over the pattern (c)

---

The convergence of the critical Dean number  $De_{cr}$  differs for the single- and two-fluid cases. In the single-fluid case, 30 basis functions in the  $r$ -direction yield convergence up to five correct decimal digits. In the two-fluid case, however, we needed 70 basis functions to obtain the third decimal digit correctly, and 100 functions to converge for the fourth one.

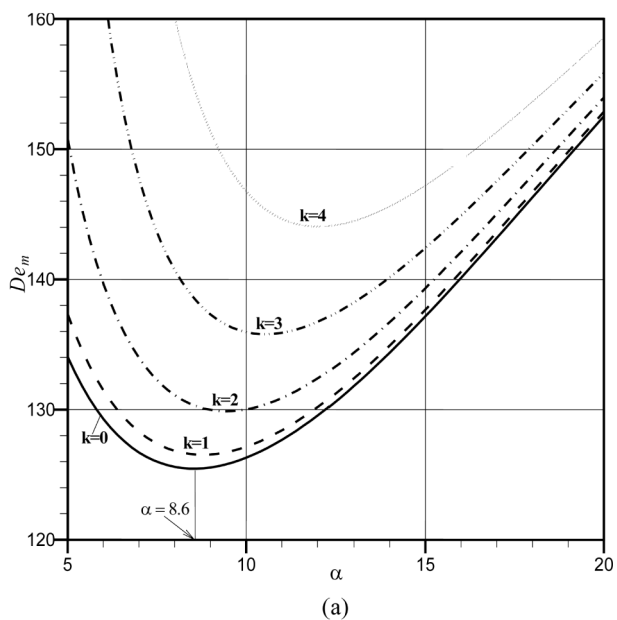
It was shown by Gelfgat *et al.* (2001c) that the most dangerous perturbation switches from axisymmetric ( $k = 0$ ) to three-dimensional ( $k \neq 0$ ) when the relative depth of the inner layer  $\bar{b}$  tends to zero or unity. This is shown in Figure 16, where the dependencies  $De_m(k, \alpha)$  for  $\bar{b} = 0.8$  and  $0.9$  are shown. At  $\bar{b} = 0.8$ , the most critical mode is axisymmetric and the critical axial wavenumber  $\alpha_{cr}$  is approximately 8.6 (Figure 16(a)). Increasing  $\bar{b}$  from 0.8 to 0.9 leads to a complete change in the perturbation pattern: the most dangerous perturbation becomes three-dimensional with  $k = 7$  and  $\alpha_{cr} \approx 39$  (Figure 16(b)). Note that in both cases shown in Figure 16, the marginal Dean numbers corresponding to some other non-critical values of  $k$  are close to the critical one. Again, this indicates the possibility of multiple axisymmetric and three-dimensional solutions in a supercritical regime.

#### 4.7 Three-dimensional instability of axisymmetric convection flows

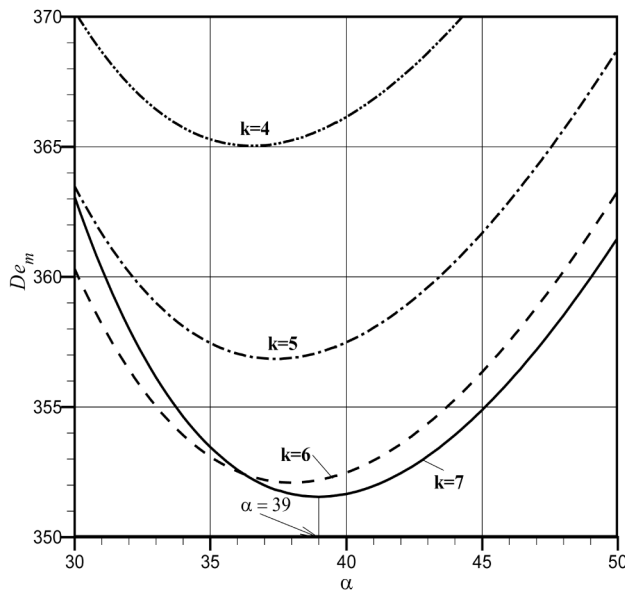
This problem was studied for convection of water ( $Pr \sim 10$ ) in Gelfgat *et al.* (1999c), and for convection of liquid metals and semiconductors ( $Pr \sim 10^{-2}$ ) in Gelfgat *et al.* (2000). The effect of an axial magnetic field on the three-dimensional instability onset was examined by Gelfgat *et al.* (2001b). The convergence of the critical Grashof number to within three decimal digits is usually reached with the use of  $30 \times 30$  basis functions in the  $r$ - and  $z$ -directions, respectively. Here, we present the stability diagram for a cylinder with a parabolically heated lateral boundary and for  $Pr = 0.03$  (Figure 17) to illustrate once more that at a certain supercriticality, say  $Gr > 3 \times 10^5$ , several modes having different azimuthal symmetry, can grow simultaneously leading to a multiplicity of the supercritical flow states.

#### 4.8 3D Taylor-Couette flow with an axial pressure gradient

An example of the computed multiple three-dimensional flows is shown in Figure 18. The problem corresponds to the experiment of Lueptow *et al.* (1992). The flow between the two cylinders, the outer cylinder is stationary and the inner one rotates, with a superimposed axial through-flow, is considered. The finite volume scheme with  $32 \times 64 \times 32$  uniformly distributed grid points in the  $r$ ,  $\theta$ , and  $z$  directions, respectively, is used for computing the flow field. In the supercritical regime, the flow approaches different asymptotic states depending on a perturbation introduced at the initial stage of the calculations (Figure 18). The numerical results are in good agreement with the experimental observations of Lueptow *et al.* (1992).



(a)



(b)

**Figure 16.**  
Two-fluid Dean flow:  
stability diagrams for  
 $\rho_{21} = \eta_{21} = 1.1$ ,  $\mathcal{A} = 10$ ,  
 $We = 100$  (a)  $\mathcal{B} = 0.8$ ,  
and (b)  $\mathcal{B} = 0.9$

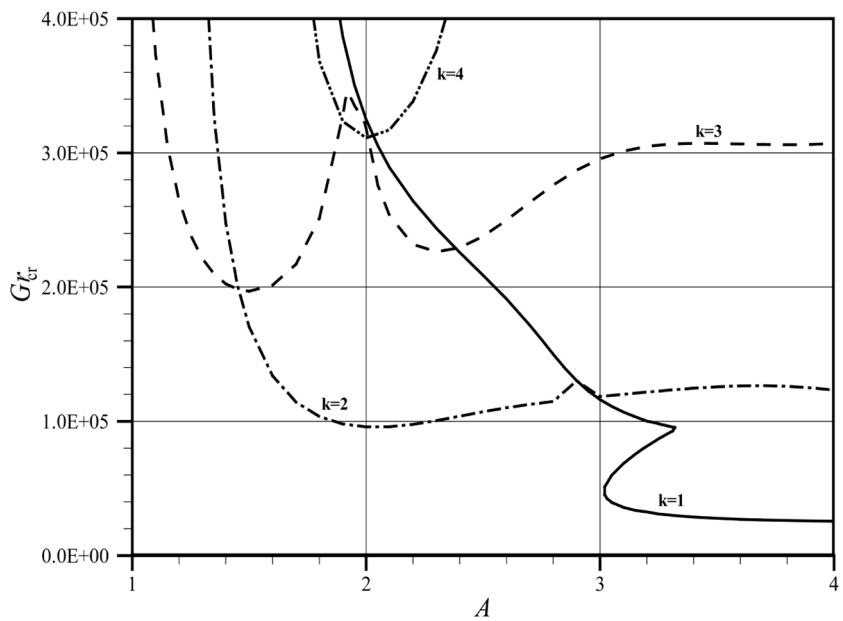
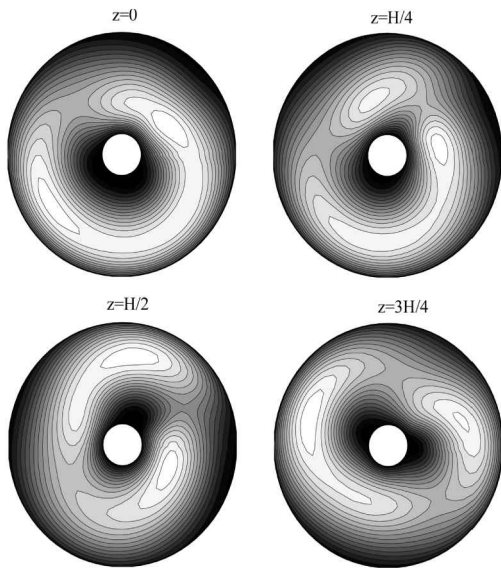


**Figure 17.**  
Stability diagram for convection in a vertical cylinder with parabolically heated sidewall (Gelfgat *et al.*, 2000).  $\text{Pr} = 0.03$ . 3D perturbations defined as  $A(r, z)\exp(ik\theta + \lambda t)$

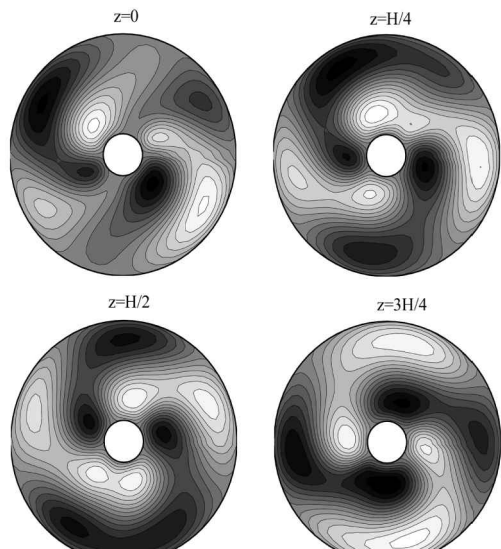
## 5. Concluding remarks

In the present review, interest lies mainly in the basic fluid phenomena, rather than in the complexities of the different processes. It has been clearly shown that despite the simplicity in the domain geometry and the assumption that the flow remains laminar, complicated multiple flow patterns are revealed in all the cases that we experienced. The most typical bifurcations observed are the turning point, Hopf and breaking of different flow symmetries such as reflectional, rotational or axial. The multiplicity of flow states observed is usually related with the breaking of symmetry and competition of different flow driving mechanisms.

Further progress in material processing will depend on the realistic large scale computational simulations because a very fine resolution is needed to resolve the various temporal and three-dimensional spatial scales involved in simulating the related unsteady flow fields. Furthermore, a large number of computations are required in parametric studies to explore the solution dependence on the process characteristic parameters. Special computational methods have to be developed to yield a reliable description of the flow behavior in such complicated processes. Such flow simulations which require extensive computer resources, pose many challenges both in terms of parallel algorithm and processing. The present global spectral Galerkin approach yields the correct pattern of the flow with a relatively few number of degrees of freedom. The explicit form



(a)



(b)

**Figure 18.**  
Multiple states of  
Taylor-Couette flow with  
axial throughflow:  
isolines of the radial  
velocity at different  
cross-sections.  $Ta = 130$ ,  
 $Re = 10$ , radii ratio is  
0.848 (out of scale on the  
graph), axial period is  
two. The initial  
perturbation is  
proportional to (a)  $\sin\theta$ ,  
and (b)  $\sin 2\theta$

of the dynamical system (2) allows for a straightforward efficient parallelization for massively parallel computer units. This gives an attractive approach to perform stability and bifurcation analyses for materials processing.

**References**

- Albensoeder, S., Kuhlmann, H.C. and Rath, H.J. (2001), "Multiplicity of steady two-dimensional flows in two-sided lid-driven cavities", *Theoret. Comput. Fluid Dynamics*, Vol. 14, pp. 223-41.
- Bartels, F. (1982), "Taylor vortices between two concentric rotating spheres", *J. Fluid Mech.*, Vol. 119, pp. 1-25.
- Bar-Yoseph, P.Z. (1994), "On multiple flow patterns and vortex breakdown phenomena in confined rotating flows", *CFD Journal*, Vol. 3, pp. 273-92.
- Bar-Yoseph, P.Z. (1995), "Confined swirling flows – a continuing challenge", in Leutloff, D. and Srivastava, R.C. (Eds), *Computational Fluid Dynamics. Selected Topics*, Springer, Berlin, pp. 257-67.
- Bar-Yoseph, P.Z., Even-Sturlesi, G., Arkadyev, A., Solan, A. and Roesner, K.G. (1992), "Mixed-convection of rotating fluids in spherical annuli", in Napolitano, M. and Sabetta, F. (Eds), *13th Int. Conf. Numer. Meth. Fluid Dyn.*, 6-10 July 1992, Rome, Lecture Notes in Physics Vol. 414, Springer, Berlin, pp. 381-5.
- Bar-Yoseph, P.Z., Solan, A., Hillen, R. and Roesner, K.G. (1990), "Taylor vortex flow between eccentric coaxial rotating spheres", *Phys. Fluids A*, Vol. 2, pp. 1564-73.
- Batchelor, G.K. (1954), "Heat transfer by free convection across a closed cavity between vertical boundaries at different temperatures", *Q. J. Appl. Math.*, Vol. 12, pp. 209-33.
- Berelowitz, M. and Bar-Yoseph, P.Z. (1992), "Finite element analysis of stirring induced by an alternating magnetic field", *Int. J. Num. Meth. Heat and Fluid Flow*, Vol. 2, pp. 155-69.
- Berger, S.A. and Talbot, L. (1983), "Flow in curved pipes", *Ann. Rev. Fluid Mech.*, Vol. 15, pp. 461-512.
- Blackburn, H.M. and Lopez, J.M. (2000), "Symmetry breaking of the flow in a cylinder driven by a rotating endwall", *Phys. Fluids*, Vol. 12, pp. 2698-701.
- Blohm, Ch. and Kuhlmann, H.C. (2002), "The two-sided lid-driven cavity: experiments on stationary and time-dependent flows", *J. Fluid Mech.*, Vol. 450, pp. 67-95.
- Cliffe, K.A. and Mullin, T. (1985), "A numerical and experimental study of anomalous modes in the Taylor experiment", *J. Fluid Mech.*, Vol. 153, pp. 243-58.
- Cliffe, K.A., Spence, A. and Tavener, S.J. (2000), "The numerical analysis of bifurcation problems with application to fluid mechanics", *Acta Numerica*, Vol. 9, pp. 39-131.
- Coles, D. (1965), "Transition in circular Couette flow", *J. Fluid Mech.*, Vol. 21, pp. 385-425.
- Crespo del Arco, E., Pulicani, J.P. and Bontoux, P. (1989), "Simulation and analysis of the time-dependent convection in low-Pr liquids", *Physico-Chemical Hydrodyn.*, Vol. 11, pp. 681-92.
- Dean, W.R. (1928), "Fluid in a curved channel", *Proc. Roy. Soc. London, Ser. A.*, Vol. 121, pp. 402-20.
- Delery, J.M. (1994), "Aspects of Vortex Breakdown", *Progr. Aerospace Sci.*, Vol. 30, pp. 1-59.
- Dijkstra, H.A. (1998), "Test problem: Rayleigh-Bénard convection", available at: <http://www.cs.kuleuven.ac.be/kurt/EUROMECH383/testproblem-en.html>
- Dold, P. and Benz, K.W. (1999), "Rotating magnetic fields: fluid flow and crystal growth applications", *Progress in Crystal Growth and Characterization of Materials*, Vol. 38, pp. 7-38.
- Erenburg, V., Gelfgat, A.Y., Kit, E., Bar-Yoseph, P.Z. and Solan, A. (2003), "Multiple states, stability and bifurcations of natural convection in rectangular cavity with partially heated vertical walls" (submitted for publication).

- Escudier, M.P. (1984), "Observation of the flow produced in a cylindrical container by a rotating endwall", *Exp. Fluids*, Vol. 2, pp. 189-96.
- Fujimura, K. and Renardy, Y.Y. (1995), "The 2:1 steady/Hopf mode interaction in the two-layer Bénard problem", *Physica D*, Vol. 85, pp. 25-65.
- Gadoin, E., Le Quéré, P. and Daube, O. (2001), "A general methodology for investigating flow instabilities in complex geometries: application to natural convection in enclosures", *Int. J. Numer. Meth. Fluids*, Vol. 37, pp. 175-208.
- Gelfgat, A.Y. (1999), "Different modes of Rayleigh-Bénard instability in two- and three-dimensional rectangular enclosures", *J. Comput. Phys.*, Vol. 156, pp. 300-24.
- Gelfgat, A.Y. (2001), "Two- and three-dimensional instabilities of confined flows: numerical study by a global Galerkin method", *CFD Journal*, Vol. 9, pp. 437-48.
- Gelfgat, A.Y. and Bar-Yoseph, P.Z. (2001), "The effect of an external magnetic field on oscillatory instability of convective flows in a rectangular cavity", *Phys. Fluids*, Vol. 13, pp. 2269-78.
- Gelfgat, A.Y. and Tanasawa, I. (1993), "Systems of basis functions for calculation of three-dimensional fluid flows in cylindrical containers with the spectral Galerkin method", *J. Institute of Industrial Science*, Vol. 45, pp. 60-3, University of Tokyo.
- Gelfgat, A.Y. and Tanasawa, I. (1994), "Numerical analysis of oscillatory instability of buoyancy convection with the Galerkin spectral method", *Numer. Heat Transfer. Pt A*, Vol. 25, pp. 627-48.
- Gelfgat, A.Y., Bar-Yoseph, P.Z. and Solan, A. (1996a), "Stability of confined swirling flow with and without vortex breakdown", *J. Fluid Mech.*, Vol. 311, pp. 1-36.
- Gelfgat, A.Y., Bar-Yoseph and Solan, A. (1996b), "Steady states and oscillatory instability of swirling flow in a cylinder with rotating top and bottom", *Phys. Fluids*, Vol. 8, pp. 2614-25.
- Gelfgat, A.Y., Bar-Yoseph, P.Z. and Solan, A. (1996c), "Confined swirling flow simulation using spectral Galerkin and finite volume methods", *Proc. 1996 ASME Fluids Engineering Division Conference*, 7-11 July 1996, FED Vol. 238, San-Diego, CA, pp. 105-11.
- Gelfgat, A.Y., Bar-Yoseph, P.Z. and Yarin, A.L. (1997), "On oscillatory instability of convective flows at low Prandtl number", *J. Fluids Eng.*, Vol. 119, pp. 823-30.
- Gelfgat, A.Y., Bar-Yoseph, P.Z. and Yarin, A.L. (1999a), "Stability of multiple steady states of convection in laterally heated cavities", *J. Fluid Mech.*, Vol. 388, pp. 315-34.
- Gelfgat, A.Y., Bar-Yoseph, P.Z. and Yarin, A.L. (1999b), "Non-symmetric convective flows in laterally heated rectangular cavities", *Int. J. Comput. Fluid Dyn.*, Vol. 11, pp. 261-73.
- Gelfgat, A.Y., Bar-Yoseph, P.Z., Solan, A. and Kowalewski, T. (1999c), "An axisymmetry-breaking instability in axially symmetric natural convection", *Int. J. Transport Phenomena*, Vol. 1, pp. 173-90.
- Gelfgat, A.Y., Bar-Yoseph, P.Z. and Solan, A. (2000), "Axisymmetry breaking instabilities of natural convection in a vertical Bridgman growth configurations", *J. Cryst. Growth*, Vol. 220, pp. 316-25.
- Gelfgat, A.Y., Bar-Yoseph, P.Z. and Solan, A. (2001a), "Three-dimensional instability of axisymmetric flow in a rotating lid - cylinder enclosure", *J. Fluid Mech.*, Vol. 438, pp. 363-77.
- Gelfgat, A.Y., Bar-Yoseph, P.Z. and Solan, A. (2001b), "Effect of axial magnetic field on three-dimensional instability of natural convection in a vertical Bridgman growth configuration", *J. Cryst. Growth*, Vol. 230, pp. 63-72.
- Gelfgat, A.Y., Yarin, A.L. and Bar-Yoseph, P.Z. (2001c), "Three-dimensional instability of a two-layer Dean flow", *Phys. Fluids*, Vol. 13, pp. 3185-95.

- Grants, I. and Gerbeth, G. (2001), "Stability of axially symmetric flow driven by a rotating magnetic field in a cylindrical cavity", *J. Fluid Mech.*, Vol. 431, pp. 407-26.
- Hurle, D.T.J. (1966), "Temperature oscillations in molten metals and their relationship to growth striae in melt-grown crystals", *Phil. Mag.*, Vol. 13, pp. 305-10.
- Jaluria, Y. (2001), "Fluid flow phenomena in materials processing – the 2000 Freeman scholar lecture", *ASME J. Fluids Engineering*, Vol. 123, pp. 173-210.
- Koschmieder, E.L. (1993), *Bénard Cells and Taylor Vortices*, Cambridge University Press, Cambridge.
- Li, J. and Renardy, Y.Y. (1998), "A numerical study of periodic disturbances on two-layer Couette flow", *Phys. Fluids*, Vol. 10, pp. 3056-71.
- Lopez, J.M., Marques, F. and Sanchez, J. (2001a), "Oscillatory modes in an enclosed swirling flow", *J. Fluid Mech.*, Vol. 439, pp. 109-29.
- Lopez, J.M., Marquez, F. and Sanchez, J. (2001b), "Oscillatory modes in an enclosed swirling flow", *J. Fluid Mech.*, Vol. 439, pp. 109-29.
- Lopez, J.M., Marques, F. and Shen, J. (2002), "An efficient spectral-projection method for the Navier-Stokes equations in cylindrical geometries. II. Three-dimensional cases", *J. Comput. Phys.*, Vol. 176, pp. 384-401.
- Lueptow, R.M., Docter, A. and Min, K. (1992), "Stability of axial flow in an annulus with a rotating inner cylinder", *Phys. Fluids*, Vol. 4, pp. 2446-55.
- Marques, F. and Lopez, J.M. (2001), "Precessing vortex breakdown mode in an enclosed cylinder flow", *Phys. Fluids*, Vol. 13, pp. 1679-82.
- Nore, C., Tuckerman, L.S., Daube, Q. and Xin, S. (2003), "The 1:2 mode interaction in exactly counter-rotating von Kármán swirling flow", (submitted for publication).
- Pallares, J., Grau, F.X. and Giralt, F. (1999), "Flow transitions in laminar Rayleigh-Bénard convection in a cubical cavity at moderate Rayleigh numbers", *Int. J. Heat Mass Transfer*, Vol. 43, pp. 753-69.
- Pallares, J., Arroyo, M.P., Grau, F.X. and Giralt, F. (2001), "Experimental laminar Rayleigh-Bénard convection in a cubical cavity at moderate Rayleigh and Prandtl numbers", *Experiments in Fluids*, Vol. 31, pp. 208-18.
- Pratte, J.M. and Hart, E. (1990), "Endwall driven, low Prandtl number convection in a shallow rectangular cavity", *J. Cryst. Growth*, Vol. 102, pp. 54-68.
- Renardy, Y.Y. and Joseph, D.D. (1985), "Couette flow of two fluids between concentric cylinders", *J. Fluid Mech.*, Vol. 150, pp. 381-94.
- Roux, B. (Ed.) (1990), "Numerical simulation of oscillatory convection in low- $\text{Pr}$  fluids: a GAMM Workshop", *Notes on Numerical Fluid Mechanics*, Vol. 27, Vieweg, Braunschweig.
- Sanchez, J., Marques, F. and Lopez, J.M. (2002), "A continuation and bifurcation technique for Navier-Stokes flows", *J. Comput. Phys.*, Vol. 180, pp. 78-98.
- Schrauf, G. (1986), "The first instability in spherical Couette-Taylor flow", *J. Fluid Mech.*, Vol. 166, pp. 287-303.
- Selver, R., Kamotani, Y. and Ostrach, S. (1998), "Natural convection of a liquid metal in vertical cylinders heated locally from the side", *J. Heat Transfer*, Vol. 120, pp. 108-14.
- Serrin, J. (1959), "Mathematical principles of classical fluid mechanics", *Handbuch der Physik*, Springer-Verlag, Berlin, pp. 126-263.
- de Vahl Davis, G. and Jones, I.P. (1983), "Natural convection in a square cavity: a comparison exercise", *Int. J. Numer. Meth. Fluids*, Vol. 3, pp. 227-48.

- Vogel, H.U. (1975), "Rückströmungblasen in Drallströmungen", *Festschrift Zum 50-jährigen Bestehen des MPI für Strömungsforschung*, Hubert, Göttingen, pp. 263-75.
- Wimmer, M. (1976), "Experiments on a viscous fluid flow between concentric rotating spheres", *J. Fluid Mech.*, Vol. 78, pp. 317-35.
- Yahata, H. (1999), "Stability analysis of natural convection in vertical cavities with lateral heating", *J. Phys. Soc. Japan*, Vol. 68, pp. 446-60.

**Further reading**

- Marques, F., Lopez, J.M. and Shen, J. (2002), "Mode interactions in an enclosed swirling flow: a double Hopf between azimuthal wavenumbers 0 and 2", *J. Fluid Mech.*, Vol. 455, pp. 263-81.